Imaging Review of the Temporal Bone: Part I. Anatomy and Inflammatory and Neoplastic Processes[1]

Amy F. Juliano, MD
Daniel T. Ginat, MD, MS
Gul Moonis, MD

From a clinical-radiologic standpoint, there are a limited number of structures and disease entities in the temporal bone with which one must be familiar in order to proficiently interpret a computed tomographic or magnetic resonance imaging study of the temporal bone. It is helpful to examine the region in an organized and systematic fashion, going through the same checklist of key structures each time. This is the first of a two-part review that provides a practical approach to understanding temporal bone anatomy, localizing a pathologic process with a focus on inflammatory and neoplastic processes, identifying pertinent positives and negatives, and formulating a differential diagnosis.

Online CME
See www.rsna.org/education/ry_cme.html

Learning Objectives:

After reading the article and taking the test, the reader will be able to:

- Identify important anatomic landmarks in the temporal bone
- Recognize clinical presentations associated with important inflammatory and neoplastic conditions in the temporal bone region
- Describe imaging features of some common inflammatory conditions in the temporal bone
- Distinguish between various tumors of the temporal bone based on CT and MR findings

Accreditation and Designation Statement

The RSNA is accredited by the Accreditation Council for Continuing Medical Education (ACCME) to provide continuing medical education for physicians. The RSNA designates this journal-based activity for a maximum of 1.0 *AMA PRA Category 1 Credit*™. Physicans should claim only the credit commensurate with the extent of their participation in the activity.

Disclosure Statement

The ACCME requires that the RSNA, as an accredited provider of CME, obtain signed disclosure statements from the authors, editors, and reviewers for this activity. For this journal-based CME activity, author disclosures are listed at the end of this article.

[1] From the Department of Radiology, Massachusetts Eye and Ear Infirmary, 243 Charles St, Boston, MA 02114. Received April 17, 2012; revision requested June 4; revision received December 14; accepted January 7, 2013; final version accepted January 29. **Address correspondence to** A.F.J. (e-mail: *amy_juliano@meei.harvard.edu*).

There are a limited number of structures and disease entities in the temporal bone with which one must be familiar in order to proficiently interpret a computed tomographic (CT) or magnetic resonance (MR) imaging study of the temporal bone. It is helpful to examine the region in an organized and systematic fashion, going through the same checklist of key structures each time.

The temporal bones comprise the lateral skull base, forming portions of the middle and posterior fossae. Each temporal bone is composed of five osseous parts: the squamous, mastoid, petrous, tympanic, and styloid portions.

Essentials

- The majority of pathologic processes occurring in the adult temporal bone are inflammatory or neoplastic in nature.
- Inflammatory conditions in the external auditory canal (EAC) include keratosis obturans, cholesteatoma, and malignant otitis externa; expansion of the canal without bone erosion suggests keratosis obturans, whereas bone erosion is characteristic of cholesteatoma and malignant otitis externa.
- The most common inflammatory conditions in the middle ear include acute and chronic otitis media, cholesterol granuloma, and cholesteatoma.
- The most common tumors in the internal auditory canal/cerebellopontine angle cistern include vestibular schwannoma and meningioma; common tumors in the middle ear include glomus tumor and facial nerve tumors extending into the middle ear cavity, such as schwannoma.
- Tumors in the EAC and mastoid region are often malignant; nonmalignant processes may cause aggressive destruction in this area, however, and should be considered as well (eg, granulomatous diseases and malignant otitis externa).

Several intrinsic channels, intrinsic fissures, and extrinsic sutures are often apparent on CT images and can mimic fractures (pseudofractures) (1). The major anatomic landmarks of the temporal bones are depicted on axial and coronal CT images (Figs 1–5) and are described in the following subsections.

Temporal Bone Anatomy

External Ear

The external ear includes the auricle and external auditory canal (EAC), which extends medially to the tympanic membrane. The tympanic membrane attaches to the tympanic annulus and measures approximately 10 mm in diameter. The normal tympanic membrane can often be faintly discerned on CT images. The lateral third of the EAC is fibrocartilagenous, while the medial two-thirds of the EAC is surrounded by the tympanic portion of the temporal bone (Fig 5). The anterior wall of the EAC also forms the posterior aspect of the glenoid fossa. The posterior wall of the EAC forms the anterior margin of the mastoid segment of the temporal bone and is resected during canal wall-down mastoidectomy.

Middle Ear and Mastoid

The middle ear is an air-filled cavity within the petrous portion of the temporal bone that contains the ossicular chain and is bounded by the tympanic membrane laterally, the inner ear structures (surrounded by the otic capsule and the cochlear promontory) medially, the tegmen tympani superiorly, and the jugular wall (floor) inferiorly (Fig 5). The scutum is a sharp bony projection to which the tympanic membrane is attached superiorly (Fig 5). The tegmen refers to a thin plate of bone that separates the dura of the middle cranial fossa from the middle ear and the mastoid cavity. The tegmen tympani is the roof of the middle ear, and the tegmen mastoideum is the roof of the mastoid (Figs 4, 5). The posterior wall of the middle ear cavity is irregular and includes the facial recess (also referred to as the facial nerve recess), pyramidal eminence, sinus tympani, and round window niche, from lateral to medial (Fig 3). The pyramidal eminence overlies the stapedius muscle, which inserts onto the head of the stapes. Another important area of the middle ear is the Prussak space (superior recess) (Fig 5). This space is marginated by the pars flaccida and scutum laterally, the lateral malleal ligament superiorly, and the neck of the malleus medially.

The middle ear can be further subdivided into the epitympanum (attic) superior to the level of the tympanic membrane, mesotympanum at the level of tympanic membrane, and hypotympanum inferior to the level of tympanic membrane (Fig 5). The hypotympanum contains the opening to the eustachian tube, with the internal carotid artery seen along its medial margin (Fig 4).

The mesotympanum contains the majority of the ossicular chain. The ossicular chain is composed of three bones: malleus (head, neck, anterior process, lateral process, and manubrium), incus (body, short process, long process, and lenticular process), and stapes (head/capitellum, anterior crus, posterior crus, and footplate) (Figs 2–5). The manubrium of the malleus is attached to the tympanic membrane, and the head of the malleus articulates with the body of the incus in the epitympanum forming the incudomalleal joint, which has a characteristic "ice cream cone" configuration on axial sections (Fig 2) (2). The lenticular process of the incus extends at approximately a right angle from the long process of the incus to articulate with the head of the stapes, forming the incudostapedial joint. The footplate of the stapes attaches to the oval window of the vestibule (Fig 5).

There are four suspensory ossicular ligaments: superior malleal, lateral

Published online
10.1148/radiol.13120733 **Content codes:** HN CT MR

Radiology 2013; 269:17–33

Abbreviations:
CPA = cerebellopontine angle
CSF = cerebrospinal fluid
DW = diffusion weighted
EAC = external auditory canal
IAC = internal auditory canal

Conflicts of interest are listed at the end of this article.

Figure 1

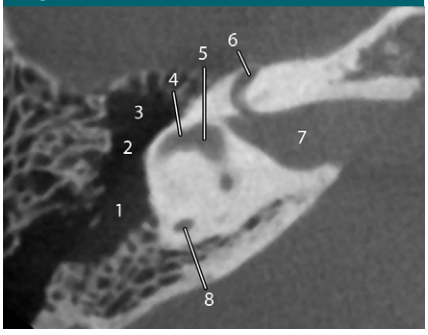

Figure 1: Axial CT image shows: *1*, mastoid antrum; *2*, aditus ad antrum; *3*, epitympanum; *4*, lateral semicircular canal; *5*, vestibule; *6*, labyrinthine segment of the facial nerve; *7*, IAC; *8*, posterior semicircular canal.

Figure 2

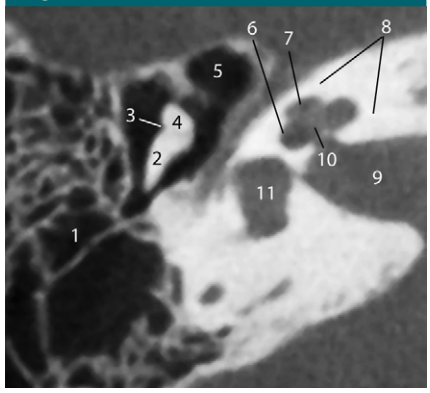

Figure 2: Axial CT image shows: *1*, mastoid air cells; *2*, incus (short process); *3*, incudomalleal joint; *4*, malleus (head); *5*, epitympanum (anterior epitympanic recess); *6*, basal turn of the cochlea; *7*, middle turn of the cochlea; *8*, otic capsule; *9*, IAC; *10*, modiolus; *11*, vestibule.

Figure 3

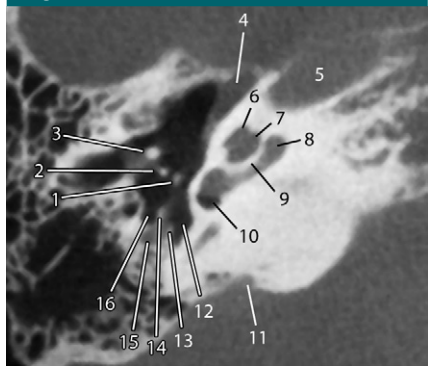

Figure 3: Axial CT image shows: *1*, stapes (head); *2*, incus (long process); *3*, malleus (neck); *4*, tensor tympani; *5*, carotid canal; *6*, apical turn of the cochlea; *7*, middle turn of the cochlea; *8*, basal turn of the cochlea; *9*, interscalar septum; *10*, round window niche; *11*, vestibular aqueduct; *12*, sinus tympani; *13*, stapedius; *14*, pyramidal eminence; *15*, mastoid portion of the facial nerve; *16*, facial recess.

Figure 4

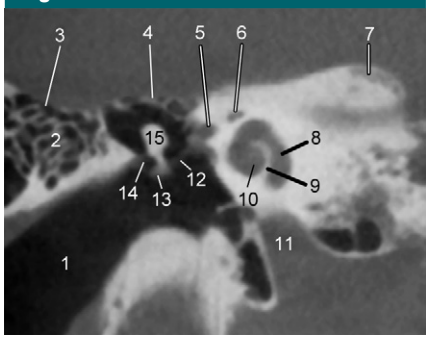

Figure 4: Coronal CT image shows: *1*, EAC; *2*, mastoid air cells; *3*, tegmen mastoideum; *4*, tegmen tympani; *5*, tympanic segment of the facial nerve; *6*, labyrinthine segment of the facial nerve; *7*, petrous apex; *8*, basal turn of the cochlea; *9*, interscalar septum; *10*, middle turn of the cochlea; *11*, carotid canal; *12*, tendon of the tensor tympani; *13*, lateral process of the malleus; *14*, lateral malleal ligament; *15*, malleus (head).

Figure 5

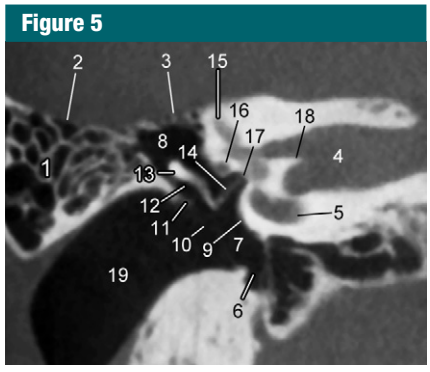

Figure 5: Coronal CT image shows: *1*, mastoid air cells; *2*, tegmen mastoideum; *3*, tegmen tympani; *4*, IAC; *5*, vestibule; *6*, hypotympanum; *7*, mesotympanum; *8*, epitympanum; *9*, cochlear promontory; *10*, tympanic membrane; *11*, scutum; *12*, Prussak space; *13*, malleus (head); *14*, stapes (crus); *15*, superior semicircular canal; *16*, tympanic segment of the facial nerve; *17*, oval window; *18*, crista falciformis; *19*, EAC.

malleal, posterior malleal, and posterior incudal. These ligaments are sometimes visible on CT images as thin linear structures. The lateral malleal ligament is most commonly identifiable among the suspensory ligaments (Fig 4) (3). The tensor tympani muscle arises from the superior surface of the cartilaginous part of the eustachian tube, courses posteriorly in the medial portion of the middle ear, turns sharply at the terminus of the cochleariform process, and attaches to the neck of the malleus (Fig 3).

The epitympanum communicates with the mastoid via the aditus ad antrum (Fig 1). Normally, the mastoid is an air-filled cavity divided into numerous compartments by mastoid septations. The mastoid air-cell size and configuration are highly variable (4). The mastoid air cells are traversed by the Koerner septum, which is a thin bony structure formed by the petrosquamous suture that extends posteriorly from the epitympanum, separating the mastoid air cells into medial and lateral compartments. The medial mastoid air cells are separated from the adjacent sigmoid sinus by the sigmoid plate.

Inner Ear

The inner ear is situated within the petrous portion and comprises the osseous labyrinth, which includes the cochlea, vestibule, and semicircular canals (Figs 2–5). The cochlea contains the end organ for hearing while the vestibule and semicircular canals are responsible for balance and equilibrium. The densest portion of the temporal bone that surrounds the osseous labyrinth is termed the otic capsule (Fig 2). The osseous labyrinth encapsulates the membranous labyrinth, which contains endolymph and is surrounded by perilymph. The structures of the membranous labyrinth (cochlear duct, utricle, saccule, semicircular ducts, and endolymphatic duct and sac) cannot be discerned at CT.

The cochlea is a spiral-shaped structure with 2 ½ to 2 ¾ turns, including the basal, middle, and apical turns, which are separated by interscalar septae (Figs 2–4). The osseous spiral lamina is a microanatomic structure that can be faintly

discerned on thin-section temporal CT images; it extends from the modiolus, paralleling the interscalar septae (5). The lateral aspect of the basal turn of the cochlea bulges into the middle ear cavity, forming the cochlear promontory (Fig 5). The nerve of Jacobson (branch of cranial nerve IX) courses over the cochlear promontory. The cochlear nerve passes from the internal auditory canal through the bony canal for the cochlear nerve (also referred to as the cochlear fossette or cochlear aperture) into the modiolus (Fig 2), which is a crown-shaped structure centered within the cochlea that transmits branches of the cochlear nerve to the organ of Corti. The organ of Corti is the end organ for hearing but is not visible on CT images.

The bony vestibule is an ovoid space located superior and posterior to the cochlea, which connects to the semicircular canals (Fig 2). There are three semicircular canals—superior, posterior, and lateral (also called horizontal)—which are oriented orthogonal to one another (Figs 1, 5). Each semicircular canal has a dilatation termed *ampulla* at one end. The posterior and superior semicircular canals share a common crus formed by the fusion of the posterior crus of the superior semicircular canal and the anterior crus of the posterior semicircular canal, which then opens into the superomedial part of the vestibule. The lateral semicircular canal, on the other hand, has two separate openings into the vestibule.

The endolymphatic duct extends from the posterior aspect of the vestibule toward the posterior cranial fossa, and ends in a blind pouch, the endolymphatic sac, at the posterior margin of the petrous ridge. The bony vestibular aqueduct (Fig 3) surrounds the endolymphatic duct and normally measures up to 1 mm at the midpoint and 2 mm at the operculum, according to the Cincinnati criteria.

The cochlear aqueduct is a narrow bony channel that surrounds the perilymphatic duct and extends from the basal turn of the cochlea, anterior to the round window, to the subarachnoid space adjacent to the pars nervosa of the jugular foramen. The cochlear aqueduct normally measures up to 0.1–0.2 mm in its midportion and is widest at the medial orifice (6).

Internal Auditory Canal

The internal auditory canal (IAC) is a channel in the petrous bone that is somewhat variable in size, shape, and orientation. The medial opening of the IAC is termed the porus acousticus. The lateral end of the IAC is termed the fundus and abuts the labyrinth. At the fundus, a transverse crest (crista falciformis) divides the IAC into superior and inferior compartments (Fig 5). A vertical crest ("Bill's bar") divides the superior compartment into anterior and posterior components. The facial nerve is located in the anterosuperior compartment, the cochlear nerve in the anteroinferior compartment, and the superior and inferior vestibular nerves in the superoposterior and inferoposterior compartments, respectively. A useful mnemonic devised for the location of the nerves in the anterior compartment is "Seven (cranial nerve VII) Up Coke (cochlear nerve) down."

Facial Nerve (Cranial Nerve VII)

Although the facial nerve itself cannot be directly visualized on CT images, its bony canal defines its course. The facial nerve exits the lateral pons, traverses the cerebellopontine angle (CPA) (cisternal segment), passes through the porus acousticus, courses through the IAC in the anterosuperior quadrant above the crista falciformis (canalicular segment), and through the petrous bone anterior to the cochlea (labyrinthine segment) to reach the geniculate ganglion (Fig 1), from which the greater superficial petrosal nerve arises. From here (anterior or first genu), the facial nerve turns posteriorly toward the medial aspect of the middle ear cavity (tympanic segment). On coronal CT images, the proximal portion of the tympanic segment and the distal portion of the labyrinthine segment of the facial nerve can be visualized superior to the cochlea, resulting in the appearance of "snake eyes" or "snail eyes" (Fig 4). The tympanic segment of the facial nerve runs inferior to the lateral semicircular canal and superolateral to the oval window (Fig 5). On MR images, enhancement is normally seen at and distal to the anterior genu of the facial nerve related to peri- and epineural venous plexuses. The intracanalicular and labyrinthine segments do not normally enhance with use of contrast material. The bone covering the tympanic segment of the facial nerve can be dehiscent, presenting a potential hazard during ossicular replacement surgery. In the posterior wall of the middle ear cavity adjacent to the facial recess, the facial nerve turns inferiorly forming the posterior or second genu. The mastoid segment of the facial nerve courses through the medial portion of the mastoid bone until it exits the skull through the stylomastoid foramen and enters the parotid gland. The chorda tympani branches off of the mastoid segment of the facial nerve and returns to the middle ear cavity via the canaliculus of the chorda tympani.

Inflammatory Lesions of the Temporal Bone

External Auditory Canal

EAC cholesteatoma.—EAC cholesteatoma is a rare lesion with an incidence of approximately 0.1%–0.5%. Most cases are spontaneous or idiopathic, although these lesions can also occur secondary to prior trauma, surgery, or radiation (7). Most patients are in an older age group and present with chronic dull pain and otorrhea, most commonly unilaterally (7). Pathologically, it is characterized by local invasion of the lining squamous epithelium of the EAC into the underlying bone, resulting in canal wall erosions and periostitis. On CT images, the lesion is characterized by focal soft tissue within the EAC (typically the inferior wall), with erosion extending into the underlying bone (Fig 6). These imaging findings are nonspecific, however, and may be mimicked by entities such as carcinoma and otitis externa. Therefore, correlation with clinical symptoms is essential.

Keratosis obturans.—Keratosis obturans represents an expansile accumulation of keratin debris within the EAC

Figure 6

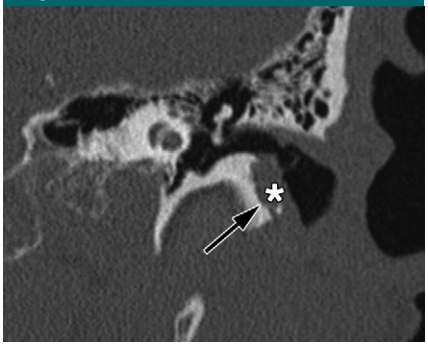

Figure 6: Coronal CT image of EAC cholesteatoma in a 73-year-old patient with a history of chronic bone erosion of the EAC. Image shows soft tissue along the inferior wall of the EAC (*), causing bone erosion (arrow).

Figure 7

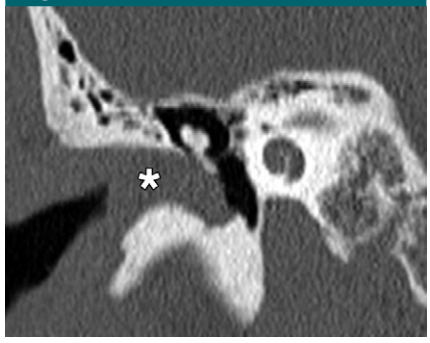

Figure 7: Coronal CT image of keratosis obturans demonstrates a soft-tissue plug in the external canal (*), with mild expansion of the canal but no bone erosion.

Figure 8

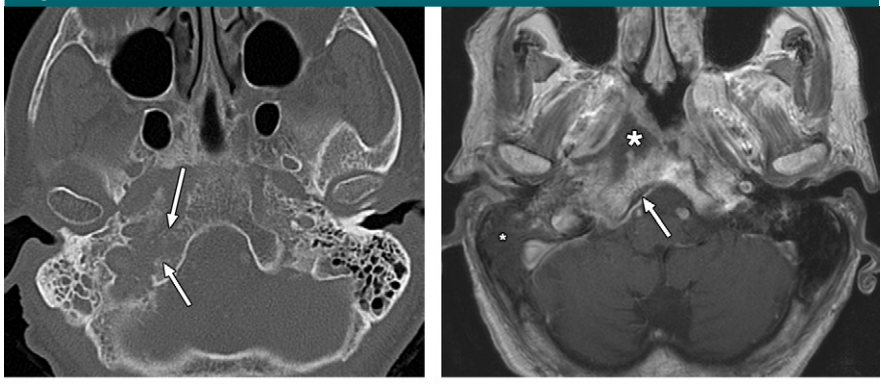

a. **b.**

Figure 8: Images of malignant otitis externa in a 93-year-old diabetic woman. **(a)** Axial CT image shows opacification of the right mastoid air cells. There are erosive changes in the petroclival region on the right (arrows). **(b)** Axial T1-weighted gadolinium-enhanced MR image in the same patient better demonstrates the prevertebral abscess (large *). There is thrombosis of the inferior petrosal sinus with a filling defect within (arrow). Notice the abnormal hypointensity in the right mastoid air cells, representing inflammatory changes (small *).

(8). In contrast to EAC cholesteatomas, it occurs in younger patients and tends to be bilateral (9). Clinically, these patients have severe pain and conductive hearing loss, with otorrhea being relatively rare. There is an association of this entity with sinusitis and bronchiectasis (8,9). On CT images, there is diffuse widening of the EAC by an epidermal plug, which may cause smooth scalloping of the surrounding bone, but there is no erosion or periostitis (Fig 7).

Malignant otitis externa.—Necrotizing or malignant otitis externa occurs most commonly in elderly diabetic patients and other patients in immunocompromised states. The patients present with severe otalgia and otorrhea, and there is a high mortality rate (10). The infection is usually caused by *Pseudomonas aeruginosa*. Clinically one sees granulation tissue in the inferior EAC at the bone-cartilaginous junction. Infection can then spread via fissures of Santorini into the soft tissues beneath the skull base, leading to skull base osteomyelitis, which can be heralded by cranial neuropathies. On images, soft-tissue thickening in the external canal is noted, often with bone destruction and inflammatory changes in the mastoid. Skull base osteomyelitis results from extension of the destructive process into the clivus, jugular foramen, and prevertebral soft tissues (Fig 8) (10). Abscesses can develop in the epidural space, brain parenchyma, and the prevertebral space as a complication. MR and CT are complementary modalities for evaluation of this entity, with the bone windows at CT showing the destructive process to greater advantage, and MR imaging better demonstrating associated soft tissue complications. The imaging differential diagnosis includes nasopharyngeal carcinoma with secondary obstruction of the eustachian tube orifice causing a secondary otomastoiditis.

Middle Ear

Acute otitis media.—Acute otitis media is primarily a disease of infants and young children. Patients present with fever, otalgia, and a red bulging tympanic membrane. The infection is usually caused by bacteria such as *Streptococcus* species or *Haemophilus influenza*. Imaging is usually not necessary in uncomplicated acute otitis media (11). If imaging is performed, one sees opacities in the middle ear and mastoid, with possible fluid levels. There is preservation of the mastoid trabeculae and the overlying cortex. Complicated mastoiditis is suggested clinically by the presence of postauricular erythema, tenderness, and edema. In this clinical situation, imaging is crucial to exclude complications, which may be intratemporal or intracranial. Coalescent mastoiditis represents destruction of the mastoid trabeculae, which may extend to the inner or outer cortex either by means of enzymatic resorption or pressure erosion of inflamed mucosa (Fig 9) (11). If there is destruction of the outer cortex of the mastoid, a subperiosteal abscess may develop within the overlying soft tissues and the patient may present with a postauricular collection (Fig 10). A Bezold abscess develops when there is bone defect at the mastoid tip medial to the insertion of the

Figure 9

Figure 9: Axial CT image of coalescent mastoiditis in a 7-year-old boy with right otalgia and fever demonstrates erosion of the inner and outer cortices of the mastoid (arrows), as well as marked demineralization of the bony septations within. Inflammatory changes are also seen within the middle ear (*).

Figure 10

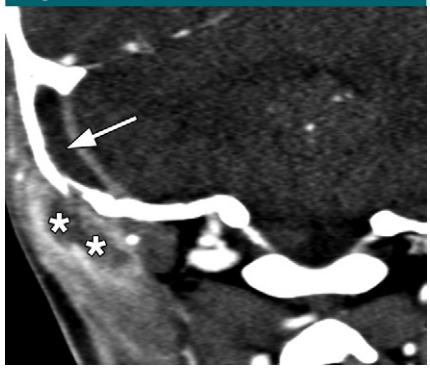

Figure 10: Coronal contrast-enhanced CT image of Bezold abscess in a 7-year-old child with acute ear infection. Image shows a rim-enhancing collection below the mastoid tip compatible with a Bezold abscess (**). Also note thrombus in the right sigmoid sinus (arrow).

Figure 11

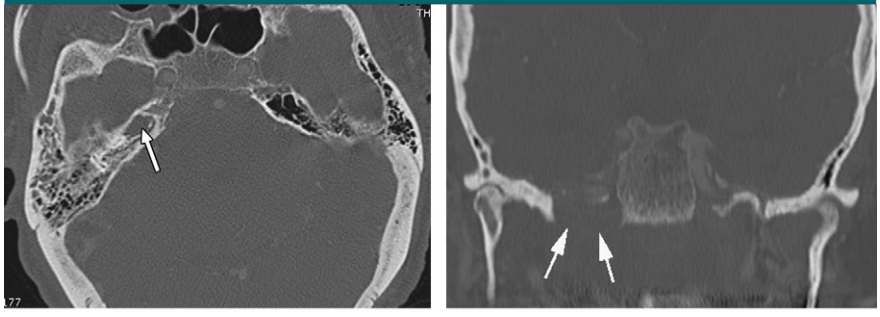

a. **b.**

Figure 11: CT images of petrous apicitis in a 78-year-old man with right ear infection. **(a)** Axial image demonstrates opacification of the right petrous apex air cells with soft-tissue attenuation (arrow). There is also scattered mastoid opacification. Note normally aerated petrous apex air cells on the left. **(b)** Coronal image better demonstrates destruction of the petrous bone (arrows).

posterior belly of the digastric muscle (digastric notch) (Fig 10). Inflammatory changes are then directed inferiorly deep to the sternocleidomastoid muscle by the fascial planes. In young children, the mastoid tip is usually not aerated; as a result, Bezold abscess in young children is uncommon (12).

When present, petrous apex air cells are connected to the mastoid air cells via numerous supra- and infralabyrinthine air channels that facilitate spread of infection from the mastoid air cells and middle ear to the petrous apex, resulting in petrous apicitis. *Streptococcus pneumonia*, *Haemophilus influenza*, and *Staphylococcus aureus* are the most common causative organisms (13). Petrous apicitis occurs in the setting of a pneumatized petrous apex (present in 30% of the population). It is characterized by septal and cortical destruction, osteitis, and adjacent meningeal inflammation. Because of the close proximity of the fifth and sixth nerves to the petrous apex, patients can develop sixth nerve palsy and deep retroorbital pain in the V1 distribution in association with otomastoiditis and petrous apicitis. This constellation of findings is termed Gradinego syndrome (14). Imaging findings include opacification of an aerated petrous apex with fluid levels and destruction of the inner septations or the cortex (Fig 11). On MR images, meningeal enhancement is better appreciated. Osteomyelitis can occur in a nonpneumatized petrous apex by means of direct medial extension of necrotizing otitis externa or by retrograde spread of thrombophlebitis along the venous plexus of the petrous carotid canal (15).

Intracranial complications of acute mastoiditis include dural venous sinus thrombosis, most commonly the sigmoid and transverse sinuses (Fig 10), epidural abscess, subdural empyema, meningitis, and brain abscess.

Chronic otitis media.—Chronic inflammation of the middle ear is known as chronic otitis media, or chronic otomastoiditis if there is mastoid involvement. It is characterized by a variety of signs, symptoms, and physical findings that result from long-term damage to the middle ear by infection and inflammation. Common mechanisms for developing chronic otitis media include underlying eustachian tube dysfunction and tympanic membrane perforation. Some of the important sequelae of chronic otitis media that may be seen at imaging include middle ear effusion, granulation tissue, cholesterol granuloma, and cholesteatoma. On CT images, all these lesions may have very similar appearances. Granulation tissue is a sequela of inflammation of the middle ear and mastoid. It encases middle ear structures but does not destroy or displace them, and there is no mass effect. Granulation tissue enhances intensely since it is highly vascularized. On gadolinium-enhanced MR images, this is readily visible. However, enhancement may be difficult to appreciate on CT images.

Cholesterol granuloma.—In the setting of eustachian tube dysfunction, there may be build-up of negative pressure or vacuum phenomenon in the middle ear cavity, leading to mucosal edema and rupture of blood vessels (13). The breakdown of erythrocytes and tissue elements release cholesterol, which incites a foreign body giant cell reaction leading to formation of a chronic

Figure 12

a. b. c.

Figure 12: Images of cholesterol granuloma. **(a)** Axial CT image in a 37-year-old woman with diplopia and headache demonstrates an expansile mass in the left petrous apex with imperceptible bone margins (arrows). **(b)** Axial T1-weighted MR image in a different patient demonstrates characteristic T1 hyperintensity in an expansile petrous apex lesion (*). **(c)** On an axial T2-weighted image (in same patient as in **b**), the lesion is heterogeneously hyperintense, with a rim of hypointensity (arrows).

Figure 13

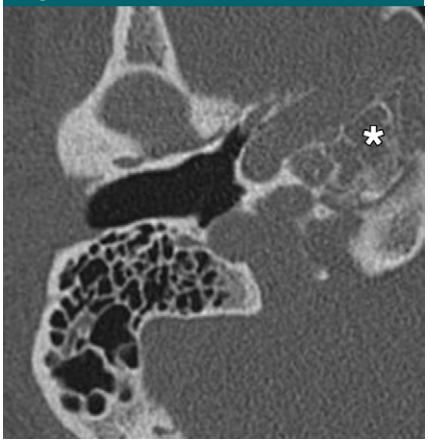

Figure 13: Axial CT image of petrous apex effusion in a 36-year-old man with right-sided sensorineural hearing loss demonstrates opacification of the pneumatized right petrous apex (*). It does not have expansile margins, distinguishing it from a petrous apex mucocele or a cholesterol granuloma. The internal septations and cortex are intact, distinguishing it from petrous apicitis.

granuloma, termed *cholesterol granuloma* (16). This lesion is also referred to as a cholesterol cyst, chocolate cyst, or blue-domed cyst. Common locations for this entity include the middle ear and the petrous apex; it can also rarely occur in a mastoidectomy cavity. In the middle ear, patients will present with a blue tympanic membrane, hemotympanum, or conductive hearing loss. In the petrous apex, these lesions may be asymptomatic or patients may have nonspecific symptoms such as vertigo, dizziness, or cranial neuropathies relating to cranial nerves V, VI, VII, and VIII. In the petrous apex, an expansile lesion with imperceptible bone margins may be seen on CT scans (Fig 12a). On MR images, the characteristic finding is the presence of intrinsic T1 shortening (hyperintensity) due to the presence of blood products (Fig 12b). On T2-weighted MR images, signal intensity is usually heterogeneously hyperintense (Fig 12c) (17). A hypointense rim on T2-weighted images may be present, which is believed to represent hemosiderin or a preserved rim of bone (18). Cholesterol granulomas do not enhance. An important differential diagnosis for this entity is entrapped simple fluid or a petrous apex effusion. However, although an effusion may mimic a cholesterol granuloma by way of MR signal characteristics, it does not cause expansion or destruction of the petrous apex air cells, a distinction that is best evaluated with CT (Fig 13).

Cholesteatoma.—Cholesteatoma is another important complication of chronic otitis media. It is characterized by accumulation of desquamated keratin epithelium in the middle ear cavity or in other pneumatized portions of the temporal bone. Histologically, choleasteatomas have two components—the acellular keratin debris, which forms the content of the sac, and the matrix, which is the biologically active component forming the sac lining. The matrix consists of an inner layer of keratinizing squamous epithelium and an outer layer of subepithelial connective tissue, also known as the perimatrix (19). The epithelial layer produces the keratin, whereas the perimatrix contains mesenchymal cells that produce proteolytic enzymes, which can resorb bone. A cholesteatoma may become secondarily infected, resulting in malodorous discharge. Most cholesteatomas are acquired (98%), with a minority (2%) being congenital. The invagination theory for the development of acquired cholesteatomas postulates the following: Chronic eustachian tube dysfunction produces a vacuum phenomenon in the middle ear cavity, leading to formation of a retraction pocket in the pars flaccida lined by surface epithelium of the tympanic membrane which grows over time (20). The epithelial invasion theory postulates ingrowth of keratinizing stratified squamous epithelium in the middle ear by means of a perforation of the tympanic membrane. Approximately 80% of acquired cholesteatomas are associated with the pars flaccida, which is the more loosely attached portion of the tympanic membrane that forms the superior one-eighth of the circumference of the drum. Approximately 20% are associated with the more tightly attached pars tensa of

Figure 14

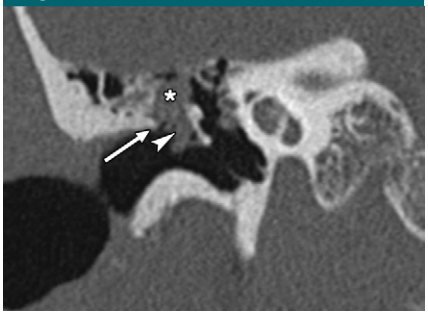

Figure 14: Coronal CT image of a pars flaccida cholesteatoma in a 56-year-old woman with a deep retraction pocket at clinical examination. Image demonstrates lobulated soft tissue in Prussak space (arrowhead) and the attic (*), displacing the ossicles medially and eroding the scutum (arrow).

Figure 15

Figure 15: Coronal CT image of a pars tensa cholesteatoma in a 31-year-old man with left-sided hearing loss and retraction pocket at clinical examination. Image demonstrates a lobulated soft-tissue mass medial to the ossicles (*), displacing the ossicles laterally. The scutum remains sharp (arrow), in contrast to that in the case of the pars flaccida cholesteatoma.

Figure 16

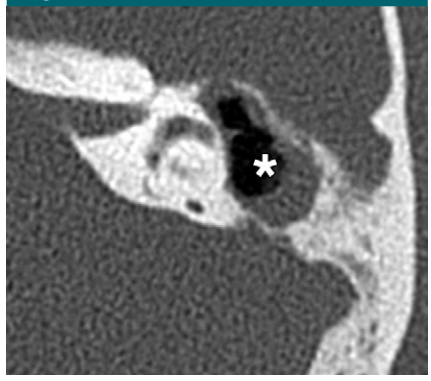

Figure 16: Axial CT image of automastoidectomy in a 51-year-old man with a history of longstanding chronic otitis media on the left. Image demonstrates a large cavity (*) in the middle ear and mastoid antrum, with nonvisualization of the ossicles. There is a small amount of residual inflammatory soft tissue. There is no history of surgery.

the tympanic membrane. Congenital cholesteatoma is postulated to arise from epithelial rests in the middle ear in a child with no previous history of otorrhea, tympanic membrane perforation, or otologic procedures. In the petrous apex, cholesteatomas can be either acquired or congenital. Both congenital and acquired cholesteatomas can be seen as a pearly white lesion at otoscopy. Clinically, patients with acquired cholesteatomas present with chronic foul-smelling otorrhea, tympanic membrane perforation, and a retraction pocket in the pars flaccida. Congenital cholesteatoma may be an incidental finding in an asymptomatic patient, or the patient may have conductive hearing loss.

CT is the imaging mainstay of temporal bone inflammation (21). Acquired pars flaccida cholesteatoma is seen as a rounded expansile lobulated lesion in the Prussak space eroding the scutum, with medial displacement and erosion of the ossicles (21) (Fig 14). The lesion may extend superiorly into the attic, and to the mastoid air cells via the aditus ad antrum. In contrast, pars tensa cholesteatoma tends to occur medial to the ossicles and displace them laterally (21) (Fig 15). Congenital cholesteatoma is commonly located in the anterior superior quadrant of the middle ear cavity just above the opening of the eustachian tube.

Some common complications of cholesteatoma include erosion of the roof of the middle ear (tegmen tympani), with or without formation of a meningoencephalocele; erosion of the bony facial canal in its tympanic or mastoid portion; and erosion of the bony covering over the lateral semicircular canal, which may result in formation of a communication between the middle ear and inner ear, also known as a labyrinthine or perilymphatic fistula. Mural cholesteatomas drain their cystic contents through the tympanic membrane into the EAC, with only the matrix lining remaining (22). This results in a characteristic "automastoidectomy" appearance, with an extensive bone destructive process in the middle ear/mastoid resembling a surgical mastoidectomy cavity (Fig 16). At MR imaging, a cholesteatoma is hypointense on T1-weighted images, is mildly hyperintense on T2-weighted images, and does not enhance (Fig 17). Reduced diffusivity may be seen on diffusion-weighted (DW) images in cholesteatomas. Non–echo-planar turbo spin-echo–based DW imaging techniques can achieve thinner sections (2 mm) with less susceptibility artifact at the air-bone interface when compared with echo-planar imaging sequences. MR imaging is also very useful in evaluating for complications such as meningoencephaloceles resulting from tegmen erosion. MR imaging can also help differentiate a recurrent cholesteatoma from cholesterol granuloma, granulation tissue, or scar (Table 1). The sensitivity of DW imaging for the detection of cholesteatomas decreases in the postoperative setting, although the specificity remains high (23).

Facial Nerve

Bell palsy.—Bell palsy refers to facial nerve paralysis with no identifiable cause. Viral inflammation, possibly prior herpes simplex virus infection, has been implicated. It is characterized by very rapid onset of facial nerve paralysis, which progresses over a few hours to up to 3 weeks. In 80% of patients symptoms improve spontaneously; if symptoms persist for more than 3 weeks, more ominous causes such as neoplasm should be investigated, and investigation should include the use of MR imaging. On imaging studies, there is enhancement of the canalicular, labyrinthine, and geniculate portions of the facial nerve (Fig 18) (23,24).

Ramsay Hunt syndrome.—Ramsay Hunt syndrome is also referred to as herpes zoster oticus. It is thought to represent reactivation of varicella zoster virus latent in the geniculate ganglion. Reactivation may occur in the setting of immunocompromised states, systemic diseases, or aging. Clinically, the patient

presents initially with burning pain in the ear; this is followed 1 day to 4 days later with vesicular eruption, facial paralysis, hearing loss, and/or vertigo. On MR images, there is enhancement of cranial nerves VII and VIII, the labyrinth, and/or the pontine facial nucleus (25).

Inner Ear

Inner ear inflammation or labyrinthitis can occur as a result of infections (viral or bacterial) or may be autoimmune or posttraumatic. Labyrinthitis ossificans is the late stage of labyrinthitis, in which there is pathologic ossification of spaces within the lumen of the bony labyrinth (comprised of the cochlea and the vestibular system). The most common region of cochlear ossification occurs in the scala tympani of the basal turn, and the most extensive cases are seen as a complication of meningitis. The evolution of labyrinthitis is characterized by three stages: acute, fibrous, and ossification (labyrinthitis ossificans) (26). In the acute stage, enhancement of the inner ear is noted on MR images, but the CT scan may appear normal. In the intermediate fibrous stage of labyrinthitis, there is loss of fluid signal intensity on heavily T2-weighted sequence images (eg, three-dimensional constructive interference in steady state [CISS] or fast imaging employing steady-state acquisition [FIESTA]), while the CT scan may still appear normal. In the late ossific stage, one sees replacement of the normal cochlea, vestibule, and/or semicircular canals by bone attenuation on CT scans (Fig 19). CT lags behind MR imaging in the detection of labyrinthitis ossificans.

Figure 17

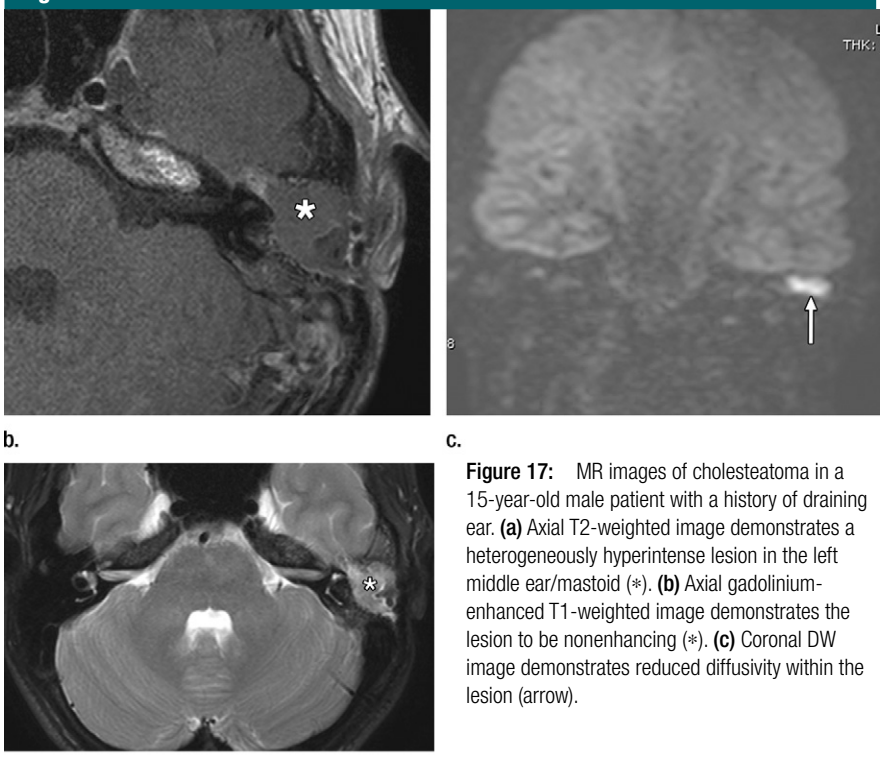

Figure 17: MR images of cholesteatoma in a 15-year-old male patient with a history of draining ear. **(a)** Axial T2-weighted image demonstrates a heterogeneously hyperintense lesion in the left middle ear/mastoid (*). **(b)** Axial gadolinium-enhanced T1-weighted image demonstrates the lesion to be nonenhancing (*). **(c)** Coronal DW image demonstrates reduced diffusivity within the lesion (arrow).

Tumors of the Temporal Bone

To assess a tumor in the temporal bone region, it is helpful to localize the lesion to one of the following areas, each of which houses a unique set of pathologic conditions: *(a)* IAC/CPA, *(b)* middle ear, *(c)* EAC and mastoid, and *(d)* petrous apex. We will consider each area separately in the following sections.

IAC/CPA

The most common masses in this area are vestibular schwannomas, meningiomas, epidermoids, and nonvestibular posterior fossa schwannomas (such as trigeminal, facial, and glossopharyngeal). Less frequently seen are arachnoid cysts, lipomas, dermoids, and malignancies such as lymphoma, melanoma, and metastases. In addition, tumors related to the petrous bone (eg, chondrosarcoma) and brain (eg, glioma) may extend into the IAC/CPA.

Vestibular schwannoma.—The most common tumor in the IAC/CPA is the vestibular schwannoma, which accounts for 60%–90% of all tumors in this region (27–29). It is also thought to be the most common intracranial nerve sheath tumor (30). Incidence is highest in the 5th through 7th decades of life (31), although they commonly present in the first 2 decades in the setting of neurofibromatosis type II, the

Table 1

MR Imaging Appearance of Temporal Bone after Surgery for Chronic Otitis Media/Cholesteatoma

Tissue Type	T1-weighted MR Imaging	T2-weighted MR Imaging	Enhancement	Diffusion Restriction
Cholesteatoma	Hypointense	Hyperintense	No	Yes
Granulation tissue	Hypointense	Hyperintense	Yes	No
Scar	Hypointense/intermediate	Hypointense/intermediate	No/delayed	No
Cholesterol granuloma	Hyperintense	Hyperintense/intermediate	No	Variable

Figure 18

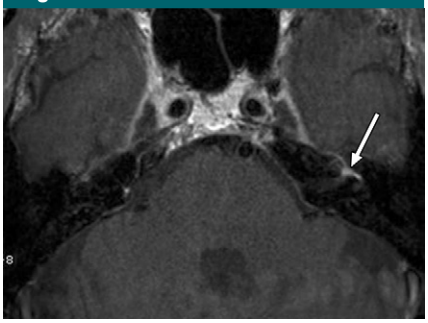

Figure 18: Axial gadolinium-enhanced T1-weighted MR image of Bell palsy in a 73-year-old man with slow-onset left facial paralysis. Images demonstrates enhancement in the first genu and proximal tympanic segment of the left facial nerve (arrow).

Figure 19

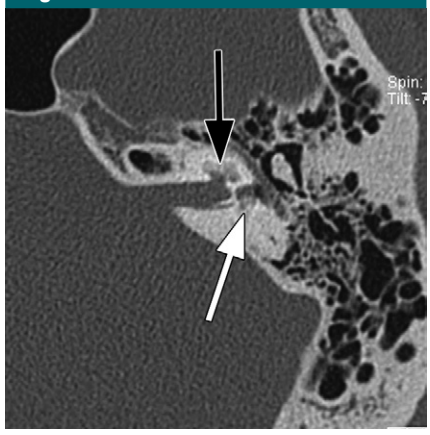

Figure 19: Axial CT image of labyrinthitis ossificans in a patient with a remote history of meningitis. Image demonstrates obliteration of the left cochlea (black arrow) and vestibule (white arrow) by sclerotic bone. Similar changes are seen on the right (not shown).

Figure 20

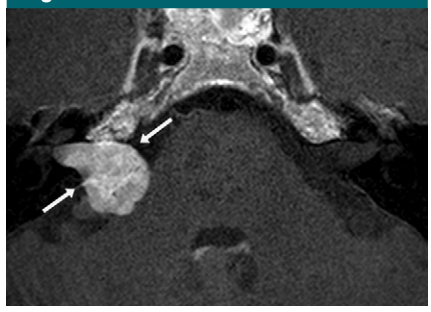

Figure 20: Axial contrast-enhanced T1-weighted MR image of vestibular schwannoma. This 51-year-old man presented with sudden asymmetric sensorineural hearing loss on the right. Image demonstrates an avidly enhancing tumor in the IAC extending through an expanded porus acousticus (between arrows) into the CPA, where it forms an acute angle with the posterior petrous ridge.

phakomatosis associated with bilateral vestibular schwannomas, multiple schwannomas of other cranial nerve origin, meningiomas, and ependymomas in the brain and spine (32). Patients present with sensorineural hearing loss, tinnitis, dysequilibrium, and/or decreased speech discrimination, secondary to pressure by the tumor on the cochlear and vestibular divisions of cranial nerve VIII (33); facial nerve manifestations are relatively uncommon (33,34). Larger tumors may compress the trigeminal nerve (causing facial numbness), the lower cranial nerves (causing cerebellar signs), or the fourth ventricle (causing hydrocephalus).

As vestibular schwannomas enlarge, they may expand medially into the CPA and laterally toward the fundus and/or into the cochlear aperture. When the former occurs, the porus may be expanded (Fig 20), and the spherical cisternal component usually forms an acute angle with the petrous bone at the bone-tumor interface (35). When a vestibular schwannoma extends into the cochlear aperture, the tumor is termed *impacted*; this finding correlates with a decreased chance of hearing preservation following surgery (36).

Most vestibular schwannomas are slow growing, with growth rates ranging from 0.2 mm to a few millimeters per year, though some may enlarge by more than 10 mm per year. Whenever feasible, surgical resection allows eradication of the tumor (37). There are three main approaches–retrosigmoid/suboccipital, middle fossa, and translabyrinthine (38–40). The latter leads to complete hearing sacrifice and is therefore generally reserved for patients with poor hearing or large tumors. Alternatively, stereotactic radiosurgery may be considered, especially in high-risk patients, those with bilateral tumors, and those with residual tumors following initial treatment (41).

On CT images, most vestibular schwannomas are isoattenuating with the cerebellum and are difficult to delineate without contrast material enhancement (28). However, if the tumor is large and causes expansion of the porus acousticus, this may be readily seen on CT bone window images, with the porus on the affected side asymmetrically wider. Calcification and hemorrhage are rare unless the tumor has been treated (42). Enhancement is usually avid and homogeneous (43), but this may be difficult to detect on CT images, especially if the tumor is small.

On MR images, schwannomas are usually iso- or mildly hypointense to brain parenchyma and hyperintense to cerebrospinal fluid (CSF) on T1-weighted images, mildly hyperintense to brain parenchyma and iso- to hypointense to CSF on T2-weighted images, and enhance avidly. Large tumors may be heterogeneous, with intra- or extramural cystic components (28), and may deform and displace the brainstem, causing parenchymal edema, and compress the fourth ventricle (Fig 21). Heavily T2-weighted sequences are helpful for outlining the tumor, as most structures except CSF appear quite dark. CSF thus provides natural contrast around the dark tumor mass (Fig 21). Heavily T2-weighted sequences may also reveal decreased signal intensity of the labyrinthine fluid ipsilateral to the tumor, thought to be related to higher protein content in the fluid (44); this may also be seen as increased signal intensity on fluid-attenuated inversion recovery images.

Meningioma.—In contrast to vestibular schwannomas, meningiomas are often eccentric to the porus acousticus, centered at the CPA; when they do extend into the IAC, they seldom expand the porus or the IAC (Fig 22). Meningiomas may extend into the middle cranial fossa by means of herniation, growth through the tentorium, or growth through the temporal bone (45,46). They may also extend into the middle ear and cavernous sinus (Fig 22b). As mentioned above, meningiomas tend to be broad-based along the posterior petrous wall, forming an obtuse angle at the bone-tumor interface, appearing either hemispherical or plaquelike (45). Dural

Figure 21

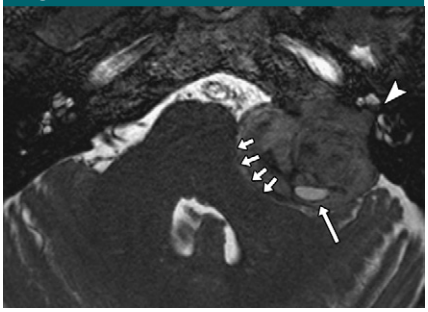

Figure 21: Axial heavily T2-weighted MR image shows a large vestibular schwannoma with an internal cyst (long arrow). It compresses the middle cerebellar peduncle and cerebellum (short arrows), with mass effect on the fourth ventricle. Laterally, there is extension into the basal turn of the cochlea (arrowhead), well depicted on this image that outlines the mass from surrounding fluid. This 55-year-old woman had left hearing loss and mild unsteadiness. This is a recurrent tumor 22 years after initial resection.

Figure 22

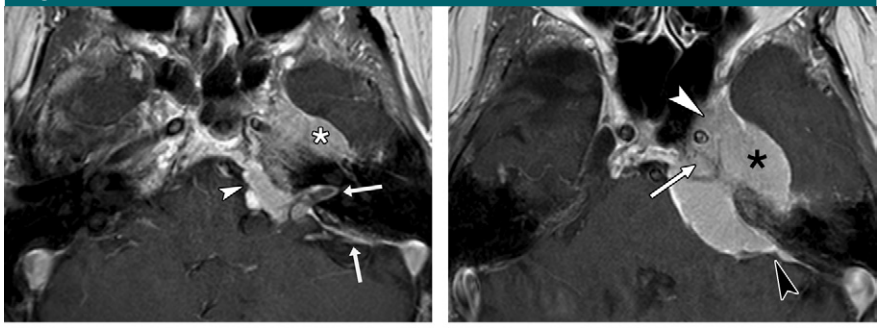

a. b.

Figure 22: Axial contrast-enhanced T1-weighted MR images of meningioma. **(a)** Image demonstrates the lesion to have a broad-based component against the posterior petrous surface (arrowhead) and an en plaque component extending into the IAC and along the posterior surface of the mastoid (arrows). The IAC is not expanded. There is extension to the middle cranial fossa (*). **(b)** Extension into the middle cranial fossa is well seen on this image from the same sequence at a more cranial level (*), along with invasion of the Meckel cave (arrow) and cavernous sinus (white arrowhead). Tumor surrounds the internal carotid artery, causing mild narrowing. Note the obtuse angles between the tumor and the bone surfaces (black arrowhead).

Figure 23

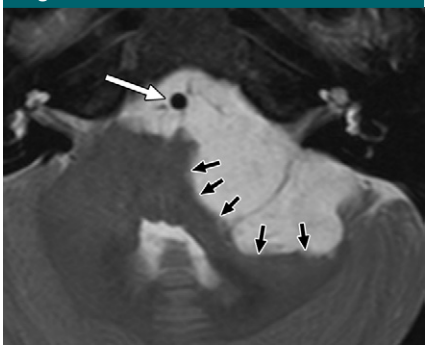

Figure 23: Axial T2-weighted MR image of epidermoid in a 40-year-old woman who presented with left sensorineural hearing loss, pressure sensation in the head worse with exertion, and tendency to drift to the left. Image shows an epidermoid in the CPA insinuating around the basilar artery (white arrow) and causing mass effect on the brainstem and cerebellum (black arrows). It does not enhance and was hyperintense on DW images (not shown). The tumor was resected by means of left suboccipital craniotomy.

enhancement extending outward from the margins of the tumor is often seen.

On CT images, meningiomas are hyper- or isoattenuating to brain parenchyma (45) and may be calcified. Sclerosis or hyperostosis in the adjacent bone may be seen. At MR imaging, meningiomas are iso- or slightly hypointense to gray matter on T1-weighted images and are iso- or hypointense to gray matter on T2-weighted images. Enhancement is usually homogeneous, unless there are calcific or cystic foci. On MR images, one might also observe surface flow voids (from marginal pial vessels) and surface CSF clefts (47–49).

Treatment is by means of surgical resection, with radiation as an adjunctive or alternative method (50). However, local recurrence is not uncommon (51).

Epidermoid.—Congenital epidermoid cysts (congenital cholesteatomas) are the third most common mass in the CPA (28,29); they consist of stratified squamous epithelial linings surrounding desquamated keratin. They are not true neoplasms and are described in detail under the earlier section, "Inflammatory Lesions." On CT images, epidermoids are similar to CSF in attenuation; if they are large, smooth remodeling of the adjacent petrous bone may be observed secondary to long-term pressure erosion. At MR imaging, they are iso- or slightly hyperintense to CSF on T1-weighted images and mildly hyperintense to CSF on T2-weighted images (Fig 23) (47). They do not enhance. On fluid-attenuated inversion recovery images, signal intensity remains hyperintense, and on DW images, an epidermoid demonstrates reduced diffusivity because of its solid nature (52). This is in contradistinction to an arachnoid cyst, which does not demonstrate diffusion reduction.

Middle Ear

When a soft-tissue mass is seen in the middle ear, a vascular structure must be excluded. This includes a persistent stapedial artery, a laterally placed or aberrant carotid artery, a carotid artery aneurysm, and an exposed dehiscent jugular bulb. True neoplasms include paraganglioma (most common); facial nerve lesions extending into the middle ear, such as schwannomas and geniculate region hemangiomas, choristomas, and perineural spread of tumor; meningiomas; adenomatous tumor of the mixed pattern type; and malignancies such as carcinomas and metastases (rare).

Most choristomas in the middle ear consist of salivary gland tissue (53,54), and they may be associated with incudostapedial or tympanic facial nerve abnormalities (55).

Adenomatous tumor of the mixed pattern type is also called middle ear adenoma (56). This is a benign tumor that does not demonstrate bone invasion. At CT, the only finding may be an opacity in the middle ear space, and this tumor may therefore be difficult to distinguish from otitis media (Fig 24). At MR imaging, it is hypointense on T1-

Figure 24

Figure 24: Coronal CT image of middle ear adenoma in a 48-year-old woman with a 6-month history of pressure sensation in the right ear. There is soft-tissue attenuation in the middle ear without adjacent bone erosion (arrow). The patient underwent tympanoplasty and biopsy of the mass and subsequent gross total resection.

Figure 25

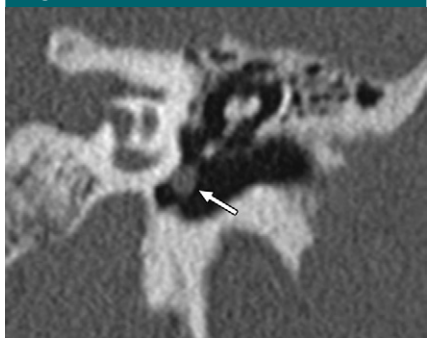

Figure 25: Coronal CT image of glomus tympanicum demonstrates a small, rounded nodule in the middle ear abutting the cochlear promontory (arrow). This 50-year-old woman had a history of chronic otitis media. At otoscopic examination, a 2-mm erythematous mass was appreciated and clinically suspected to represent a glomus tympanicum.

weighted images, hyperintense on T2-weighted images, and enhances with contrast material administration.

Paraganglioma.—Tumors of paraganglia cells are termed *paragangliomas*, but in the head and neck region, the term *glomus tumor* has been used ever since discovery of the paraganglion located in the adventitia of the dome of the jugular bulb by Guild in 1941, who named it glomus jugularis (57). Paraganglioma is the second most common tumor involving the temporal bone (28). Glomus tumors in the temporal bone region arise from the jugulotympanic paraganglia along the nerves of Jacobson and Arnold (tympanic branch of the glossopharyngeal nerve and auricular branch of the vagus nerve, respectively). Glomus tympanicum refers to those confined to the tympanic cavity (arising from paranglia cells along the nerve of Jacobson) and glomus jugulare refers to those tumors involving the jugular bulb and the base of skull (arising from paraganglia cells along the nerve of Jacobson or Arnold). Glomus jugulotympanicum has components in both the middle ear and the jugular foramen.

Jugulotympanic paragangliomas occur three to four times more often in women than in men. Patients typically present between the 4th and 6th decades of life. Up to 10% of patients may have multiple paragangliomas, so it behooves the radiologist to continue the search for additional lesions when interpreting a study, whether in the temporal bones, skull base, or neck (58). Paragangliomas are seen in a familial form in multiple endocrine neoplasia (MEN) 2a and 2b. These tumors are slow growing and locally infiltrating, growing along planes of least resistance in existing pathways in the temporal bone, and they rarely metastasize. Most patients present with otologic concerns (conductive hearing loss, pulsatile tinnitis, or a retrotympanic mass) (58,59).

Paragangliomas are highly vascular and therefore enhance avidly. Glomus tympanicum paragangliomas are found against the cochlear promontory and are usually small at presentation since they cause otologic symptoms early on (Fig 25) (60,61). It is important to inspect the margins of the jugular foramen to exclude a glomus jugulotympanicum; localized lytic or permeative bone destruction is characteristic of a glomus tumor involving the jugular foramen, and is well seen on CT scans (Fig 26a) (62).

The soft-tissue mass itself is better appreciated on MR images, showing avid enhancement. In larger tumors, a "salt-and-pepper" appearance may be visible on T1- and T2-weighted MR images (Fig 26b) (63). Multiple internal tumoral vessels manifest as serpentine and arborizing flow voids.

At angiography, enlarged feeding arteries and rapidly draining veins may be seen (64). In tympanicum tumors, blood loss is minimal, and preoperative embolization is not indicated. However, preoperative angiography and embolization of larger jugulotympanicum tumors are commonly performed to help reduce intraoperative blood loss.

Indium 111 octreotide is useful for detecting multicentric, metastatic, or recurrent tumors. The sensitivity of iodine 123–metaiodobenzylguanidine for head and neck paragangliomas is lower (65–67).

EAC and Mastoid

Tumors in the EAC and mastoid region are often malignant, with squamous cell carcinoma being by far the most common (27). Patients with EAC squamous cell carcinoma frequently have a long history of chronic ear infections. There is aggressive bone destruction, and there may be invasion of surrounding soft tissues including intracranial, inframastoid, middle ear, parotid, carotid, and temporomandibular joint involvement (Fig 27) (68–70). Other malignancies such as basal cell carcinoma, melanoma, lymphoma, myeloma, metastases, chondrosarcoma, and osteosarcoma occur much less frequently.

Aggressive bone destruction may be seen with some benign processes and should be considered in the differential diagnosis. These include granulomatous diseases such as Langerhans cell histiocytosis (Fig 28), tuberculosis, and Wegener granulomatosis. Aggressive infections such as malignant otitis externa and radiation necrosis are additional considerations.

Petrous Apex

True neoplasms in the petrous apex include chondrosarcoma, chordoma, osteosarcoma, and meningioma. Myeloma, lymphoma, and metastases may also occur. The petrous area may be secondarily involved by regional tumors such as trigeminal schwannoma, jugular paraganglioma, and nasopharyngeal carcinoma. The latter is usually seen along

Figure 26

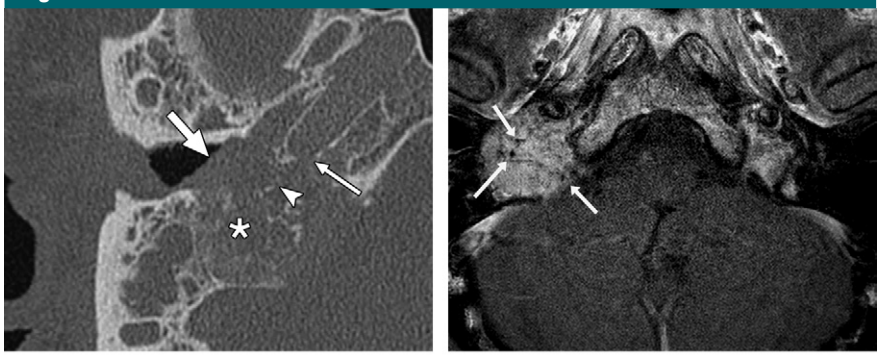

a. b.

Figure 26: Images of glomus jugulotympanicum. **(a)** Axial CT image demonstrates the moth-eaten, permeative bone destruction around the tumor. On this image through the right temporal bone, one can appreciate destruction of the margins of the jugular foramen (*), the caroticojugular spine (arrowhead), and the carotid canal (small arrow). Note the tumor extending into the middle ear (large arrow). **(b)** Axial contrast-enhanced T1-weighted MR image shows the large enhancing tumor with internal flow voids (arrows), creating the so-called salt-and-pepper appearance. This patient initially presented at age 56 years with right ear fullness, hearing loss, and audible whooshing sound that correlated with heart beat. Over the next 4 years, the tumor gradually enlarged, with new right true vocal cord paralysis indicating new involvement of the vagus nerve. He underwent proton beam radiation therapy.

Figure 27

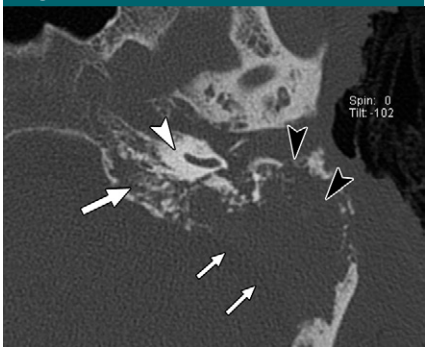

Figure 27: Axial CT image of squamous cell carcinoma of the EAC with extension to the mastoid. Patient was a 64-year-old woman with recurrent and persistent left ear infection not improved with antibiotics; biopsy revealed the diagnosis. CT image demonstrates extensive bone destruction involving the EAC margin and mastoid (black arrowheads), extending to the petrous apex (large arrow). The dense otic capsule is relatively spared (white arrowhead). Abnormal soft tissue fills the EAC, middle ear, and mastoid, extending into the posterior cranial fossa (small arrows). The auricle is also thickened, with ulcerated margins.

Figure 28

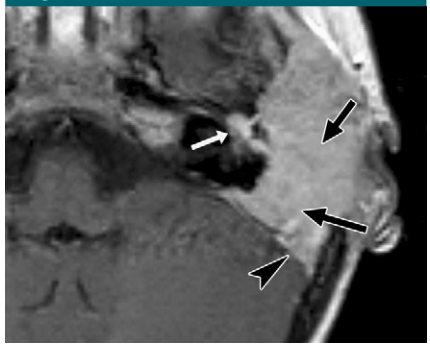

Figure 28: Axial contrast-enhanced T1-weighted MR image of Langherhans cell histiocytosis shows solid enhancing tissue involving the EAC and mastoid (black arrows). There is also involvement of the middle ear (white arrow) and sigmoid sinus (arrowhead). Patient was a 2-year-old boy with otitis media starting at 8 months of age, now with pus and bloody discharge and diffuse swelling in the ear region. Biopsy revealed Langherhans cell histiocytosis.

the petrooccipital fissure, superior to the fossa of Rosenmüller. Unlike lesions in the IAC and middle ear, lesions in the petrous apex usually reach considerable size before causing symptoms.

Chondrosarcoma.—Chondrosarcoma is the most common primary malignancy to involve the petrous apex. These tumors tend to occur along the petrosphenoidal and petrooccipital synchondroses, off midline. Occasionally, however, chordomas, which arise from notochordal remnants and are typically seen in the midline, may be found off midline as well and may mimic a chondrosarcoma radiologically (71,72). Additionally, the chondroid subtype of chordoma may be difficult to distinguish from the myxoid variant of chondrosarcoma pathologically (73).

Figure 29

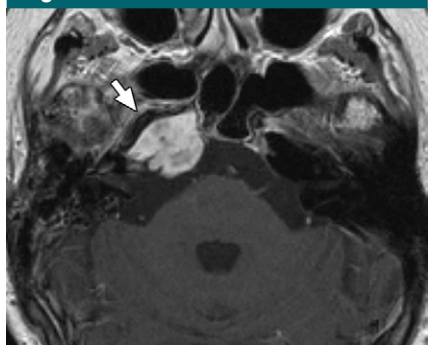

Figure 29: Axial contrast-enhanced T1-weighted MR image of petrous apex chondrosarcoma. Image shows the tumor mass in the petrous apex causing displacement of the petrous carotid artery (arrow). It was hyperintense on T2-weighted images (not shown) and enhances avidly.

At CT, these tumors enhance mildly to moderately, may contain calcifications, and cause surrounding bone destruction (71,74,75). At MR imaging, the lesions are hypointense on T1-weighted images and hyperintense on T2-weighted images, although their appearance may be quite heterogeneous (71,75,76). Enhancement is marked but may also be heterogeneous (Fig 29).

Endolymphatic sac tumor.—Endolymphatic sac tumor is a locally invasive papillary cystadenomatous tumor (56,77,78). Most cases are sporadic, although a minority may be seen in the setting of von Hippel-Lindau disease (7%) (79). The tumor causes local bone destruction in the region of the vestibular aqueduct in the retrolabyrinthine petrous bone.

At CT, the bone invaded by tumor has a moth-eaten, lytic appearance, with intratumoral bone spicules often seen (Fig 30a). At MR imaging, areas of intrinsic T1 shortening are commonly seen, reflecting blood products (Fig 30b). Low-signal-intensity areas may

represent hemosiderin. Enhancement is usually heterogeneous (80).

Facial Nerve

The most common benign tumors of the facial nerve are schwannomas and hemangiomas. The most important consideration in the malignant category is perineural spread of tumor along the facial nerve.

Facial schwannoma.—Facial nerve schwannomas can involve any segment of the nerve and may span multiple segments (81). The geniculate ganglion is frequently involved (82). Of note, only a minority of patients initially present with facial palsy; many have no facial nerve symptoms at all (82). Facial nerve schwannomas in the IAC/CPA typically manifest as sensorineural hearing loss, presumably because the thinly myelinated sensory fibers of cranial nerve VIII are more sensitive to compressive effects by the tumor than are the thickly myelinated motor fibers of the facial nerve (82). Facial schwannomas in the geniculate region can grow into the middle cranial fossa. Those along the tympanic segment may bulge into the middle ear and compress the ossicular chain, causing conductive hearing loss. Those in the mastoid segment are more likely to present with facial palsy, owing to the surrounding narrow bony canal exerting pressure on the growing tumor (82). Those in the parotid segment present as painless neck masses (83).

At CT, the tumor may be seen to cause expansile smooth remodeling of the surrounding bony canal. At MR imaging, an expansile, enhancing mass can be appreciated (Fig 31). It may have a tubular appearance, may span multiple segments, or may have a sausage-link appearance, with areas that are relatively narrower between "links" that are expansile. In the IAC, they may be indistinguishable from vestibular schwannomas (84,85). In the geniculate ganglion region, differential diagnostic considerations include hemangioma and meningioma, although these lesions tend to demonstrate intratumoral bone spicules.

Hemangioma.—Hemangiomas may be seen along the intratemporal course of the facial nerve, most often in the region of the geniculate ganglion, followed by the IAC, and are seen least often at the posterior genu. These tumors often grow among bone trabeculae and may form bone; in these cases the term *ossifying hemangioma* is sometimes used (86). Recent literature suggests that these lesions are, in fact, venous malformations (87). These lesions characteristically have an expansile honeycomb appearance and may demonstrate intratumoral bone spicules on CT images (Fig 32a) (88). These may be difficult to distinguish from meningiomas with intraosseous involvement. On MR images, there may be heterogeneous signal intensities and avid enhancement (Fig 32b).

Perineural spread of tumor.—With segmental facial nerve thickening and enhancement, an important malignant process to consider is perineural spread of tumor (Fig 33a). The source of malignancy is usually the parotid gland, for example, adenoid cystic carcinoma (Fig 33b) or mucoepidermoid carcinoma, or a nearby skin malignancy that secondarily invades or metastasizes to the parotid gland (89,90). Tumor burden can vary along the course of the nerve, resulting in varying degrees of thickening

Figure 30

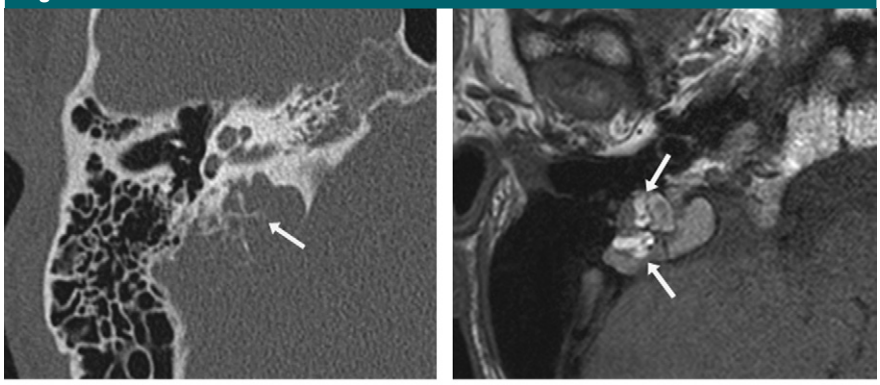

a. b.

Figure 30: Images of endolymphatic sac tumor in a 46-year-old man who presented at the emergency room with acute onset of vertigo. **(a)** Axial CT image demonstrates an expansile lesion causing lytic bone destruction, centered around the vestibular aqueduct. Intratumoral spicules can be seen (arrow). **(b)** On nonenhanced T1-weighted MR image, areas of intrinsic T1 shortening are quite characteristic of this tumor (arrows). The tumor was resected by means of a translabyrinthine approach.

Figure 31

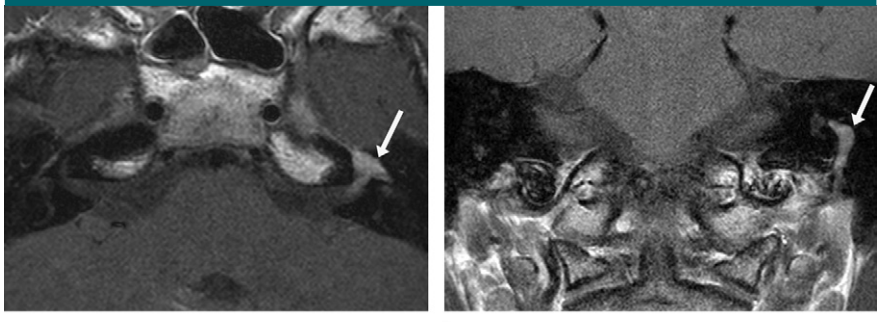

a. b.

Figure 31: Contrast-enhanced T1-weighted MR images of facial nerve schwannoma in a 35-year-old man who developed acute onset left facial paralysis. **(a)** On axial image, an expansile, enhancing tumor involves the distal labyrinthine, geniculate, and tympanic segments (arrow) of the facial nerve. **(b)** Coronal image shows that the posterior genu and mastoid segments are also involved (arrow).

Figure 32

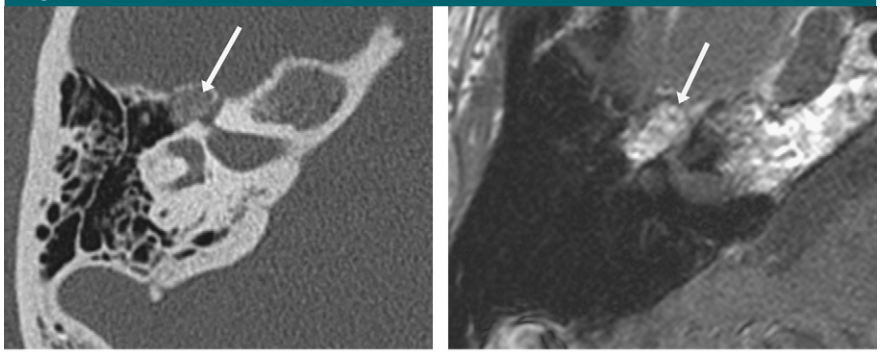

a. b.

Figure 32: Images of hemangioma in the geniculate region in a 48-year-old woman with new right facial fasciculation in the region of the right eye, progressing to the lower face, and then global weakness of the right face with synkinesis. **(a)** Axial CT image demonstrates an expansile mass with intratumoral bone spicules (arrow) in the region of the geniculate ganglion. **(b)** On contrast-enhanced axial T1-weighted MR image, avid enhancement can be seen (arrow).

Figure 33

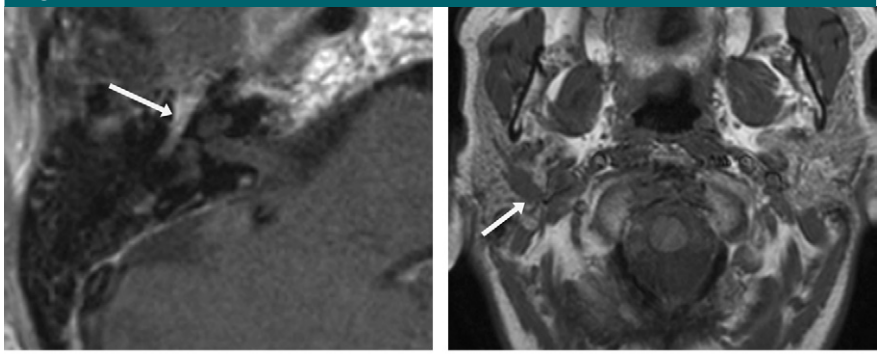

a. b.

Figure 33: Axial T1-weighted MR images show perineural spread of tumor along the facial nerve in a 58-year-old woman with transient lower lip numbness and weakness. **(a)** Contrast-enhanced image shows expansile enhancement involving the geniculate ganglion and tympanic segment of the facial nerve (arrow). The mastoid segment is involved as well (not shown). **(b)** Nonenhanced image more caudally reveals an adenoid cystic carcinoma in the right parotid gland that extends to the stylomastoid foramen (arrow) as the source; it was subsequently resected.

and enhancement; "skip lesions" may be seen where there are areas of uninvolved nerve between abnormal segments (91). It is important to note that the original tumor at the primary site could be absent if it has been treated; this does not preclude the diagnostic consideration of active perineural spread detectable at imaging.

Conclusion

In this review, we highlighted the major anatomic landmarks in the temporal bone one should be familiar with to be able to describe normal and pathologic findings and provide an interpretation. We described the most frequently encountered pathologic conditions in various locations of the temporal bone, with a focus on inflammatory and neoplastic processes (Table 2). CT and MR are the major tools for imaging evaluation. CT offers excellent delineation of soft-tissue abnormalities against a background of air (middle ear cavity, EAC, mastoid air cells) and allows assessment of bone changes and/or involvement. MR imaging offers more detailed characterization of soft tissue and fluid, allows better visualization of enhancement in small structures, and aids in distinction between soft tissues of different nature (eg, granulation tissue versus tumor).

Disclosures of Conflicts of Interest: A.F.J. No relevant conflicts of interest to disclose. **D.T.G.** No relevant conflicts of interest to disclose. **G.M.** No relevant conflicts of interest to disclose.

References

1. Collins JM, Krishnamoorthy AK, Kubal WS, Johnson MH, Poon CS. Multidetector CT of temporal bone fractures. Semin Ultrasound CT MR 2012;33(5):418–431.

Table 2

Inflammatory and Neoplastic Processes by Location

Location	Inflammatory	Neoplastic
EAC/mastoid	Cholesteatoma; keratosis obturans; malignant otitis externa	Squamous cell carcinoma; other malignancies
Middle ear	Otitis media; cholesterol granuloma; congenital cholesteatoma; acquired cholesteatoma	Glomus tympanicum/jugulotympanicum; adenoma; choristoma
Facial nerve	Bell palsy; Ramsay-Hunt	Schwannoma; hemangioma (geniculate); meningioma (geniculate); perineural spread of tumor
Petrous apex	Petrous apicitis; cholesterol granuloma; cholesteatoma	Meningioma; chondrosarcoma; osteosarcoma; chordoma; endolymphatic sac tumor; metastasis; direct extension from nasopharyngeal carcinoma

2. Stephan AL, Isaacson JE. Incudomalleolar joint separation. Am J Otol 2000;21(2):284–285.
3. Lemmerling MM, Stambuk HE, Mancuso AA, Antonelli PJ, Kubilis PS. CT of the normal suspensory ligaments of the ossicles in the middle ear. AJNR Am J Neuroradiol 1997;18(3):471–477.
4. Virapongse C, Sarwar M, Bhimani S, Sasaki C, Shapiro R. Computed tomography of temporal bone pneumatization. I. Normal pattern and morphology. AJR Am J Roentgenol 1985;145(3):473–481.
5. Fatterpekar GM, Doshi AH, Dugar M, Delman BN, Naidich TP, Som PM. Role of 3D CT in the evaluation of the temporal bone. RadioGraphics 2006;26(Suppl 1):S117–S132.
6. Mukherji SK, Baggett HC, Alley J, Carrasco VH. Enlarged cochlear aqueduct. AJNR Am J Neuroradiol 1998;19(2):330–332.
7. Dubach P, Häusler R. External auditory canal cholesteatoma: reassessment of and amendments to its categorization, pathogenesis, and treatment in 34 patients. Otol Neurotol 2008;29(7):941–948.
8. Piepergerdes MC, Kramer BM, Behnke EE. Keratosis obturans and external auditory canal cholesteatoma. Laryngoscope 1980; 90(3):383–391.
9. Tran LP, Grundfast KM, Selesnick SH. Benign lesions of the external auditory canal. Otolaryngol Clin North Am 1996;29(5): 807–825.
10. Carfrae MJ, Kesser BW. Malignant otitis externa. Otolaryngol Clin North Am 2008; 41(3):537–549, viii–ix.
11. Vazquez E, Castellote A, Piqueras J, et al. Imaging of complications of acute mastoiditis in children. RadioGraphics 2003;23(2): 359–372.
12. Marioni G, de Filippis C, Tregnaghi A, Marchese-Ragona R, Staffieri A. Bezold's abscess in children: case report and review of the literature. Int J Pediatr Otorhinolaryngol 2001;61(2):173–177.
13. Razek AA, Huang BY. Lesions of the petrous apex: classification and findings at CT and MR imaging. RadioGraphics 2012;32(1): 151–173.
14. Schmalfuss IM. Petrous apex. Neuroimaging Clin N Am 2009;19(3):367–391.
15. Connor SE, Leung R, Natas S. Imaging of the petrous apex: a pictorial review. Br J Radiol 2008;81(965):427–435.
16. Tringali S, Linthicum FH Jr. Cholesterol granuloma of the petrous apex. Otol Neurotol 2010;31(9):1518–1519.
17. Pisaneschi MJ, Langer B. Congenital cholesteatoma and cholesterol granuloma of the temporal bone: role of magnetic resonance imaging. Top Magn Reson Imaging 2000;11(2):87–97.
18. Hoeffner EG. Temporal bone imaging. New York, NY: Thieme, 2008.
19. Dornelles C, Meurer L, Selaimen da Costa S, Schweiger C. Histologic description of acquired cholesteatomas: comparison between children and adults. Braz J Otorhinolaryngol 2006;72(5):641–648.
20. Semaan MT, Megerian CA. The pathophysiology of cholesteatoma. Otolaryngol Clin North Am 2006;39(6):1143–1159.
21. Baráth K, Huber AM, Stämpfli P, Varga Z, Kollias S. Neuroradiology of cholesteatomas. AJNR Am J Neuroradiol 2011;32(2):221–229.
22. Nardis PF, Teramo M, Giunta S, Bellelli A. Unusual cholesteatoma shell: CT findings. J Comput Assist Tomogr 1988;12(6):1084–1085.
23. Vercruysse JP, De Foer B, Pouillon M, Somers T, Casselman J, Offeciers E. The value of diffusion-weighted MR imaging in the diagnosis of primary acquired and residual cholesteatoma: a surgical verified study of 100 patients. Eur Radiol 2006;16(7):1461–1467.
24. Martin-Duverneuil N, Sola-Martínez MT, Miaux Y, et al. Contrast enhancement of the facial nerve on MRI: normal or pathological? Neuroradiology 1997;39(3):207–212.
25. Sartoretti-Schefer S, Kollias S, Valavanis A. Ramsay Hunt syndrome associated with brain stem enhancement. AJNR Am J Neuroradiol 1999;20(2):278–280.
26. Paparella MM, Sugiura S. The pathology of suppurative labyrinthitis. Ann Otol Rhinol Laryngol 1967;76(3):554–586.
27. Schuknecht HF. Pathology of the ear. Cambridge, Mass: Harvard University Press, 1974.
28. Valavanis A, Schubiger O, Naidich TP. Clinical imaging of the cerebello-pontine angle. Berlin, Germany: Springer-Verlag, 1987.
29. Brackmann DE, Bartels LJ. Rare tumors of the cerebellopontine angle. Otolaryngol Head Neck Surg (1979) 1980;88(5):555–559.
30. Levin VA. Cancer in the nervous system. New York, NY: Churchill Livingstone, 1996.
31. Propp JM, McCarthy BJ, Davis FG, Preston-Martin S. Descriptive epidemiology of vestibular schwannomas. Neuro-oncol 2006; 8(1):1–11.
32. Martuza RL, Ojemann RG. Bilateral acoustic neuromas: clinical aspects, pathogenesis, and treatment. Neurosurgery 1982;10(1):1–12.
33. Selesnick SH, Jackler RK. Clinical manifestations and audiologic diagnosis of acoustic neuromas. Otolaryngol Clin North Am 1992; 25(3):521–551.
34. Hart RG, Gardner DP, Howieson J. Acoustic tumors: atypical features and recent diagnostic tests. Neurology 1983;33(2):211–221.
35. Hatam A, Bergström M, Möller A, Olivecrona H. Early contrast enhancement of acoustic neuroma. Neuroradiology 1978;17(1):31–33.
36. Dubrulle F, Ernst O, Vincent C, Vaneecloo FM, Lejeune JP, Lemaitre L. Cochlear fossa enhancement at MR evaluation of vestibular Schwannoma: correlation with success at hearing-preservation surgery. Radiology 2000; 215(2):458–462.
37. National Institutes of Health Consensus Development Conference Statement on Acoustic Neuroma, December 11-13, 1991. The Consensus Development Panel. Arch Neurol 1994;51(2):201–207.
38. Cohen NL, Hammerschlag P, Berg H, Ransohoff J. Acoustic neuroma surgery: an eclectic approach with emphasis on preservation of hearing—the New York University-Bellevue experience. Ann Otol Rhinol Laryngol 1986;95(1 Pt 1):21–27.
39. Harner SG, Ebersold MJ. Management of acoustic neuromas, 1978-1983. J Neurosurg 1985;63(2):175–179.
40. Glasscock ME 3rd, Kveton JF, Jackson CG, Levine SC, McKennan KX. A systematic approach to the surgical management of acoustic neuroma. Laryngoscope 1986;96(10): 1088–1094.
41. Norén G, Arndt J, Hindmarsh T. Stereotactic radiosurgery in cases of acoustic neurinoma: further experiences. Neurosurgery 1983; 13(1):12–22.
42. Castillo R, Watts C, Pulliam M. Sudden hemorrhage in an acoustic neuroma: case report. J Neurosurg 1982;56(3):417–419.
43. Möller A, Hatam A, Olivecrona H. Diagnosis of acoustic neuroma with computed tomography. Neuroradiology 1978;17(1):25–30.
44. Somers T, Casselman J, de Ceulaer G, Govaerts P, Offeciers E. Prognostic value of magnetic resonance imaging findings in hearing preservation surgery for vestibular schwannoma. Otol Neurotol 2001;22(1):87–94.
45. Valavanis A, Schubiger O, Hayek J, Pouliadis G. CT of meningiomas on the posterior surface of the petrous bone. Neuroradiology 1981; 22(3):111–121.
46. Naidich TP, Lin JP, Leeds NE, Pudlowski RM, Naidich JB. Primary tumors and other masses of the cerebellum and fourth ventricle: differential diagnosis by computed tomography. Neuroradiology 1977;14(4):153–174.
47. Gentry LR, Jacoby CG, Turski PA, Houston LW, Strother CM, Sackett JF. Cerebellopontine angle-petromastoid mass lesions: compara-

tive study of diagnosis with MR imaging and CT. Radiology 1987;162(2):513–520.

48. Spagnoli MV, Goldberg HI, Grossman RI, et al. Intracranial meningiomas: high-field MR imaging. Radiology 1986;161(2):369–375.
49. Zimmerman RD, Fleming CA, Saint-Louis LA, Lee BC, Manning JJ, Deck MD. Magnetic resonance imaging of meningiomas. AJNR Am J Neuroradiol 1985;6(2):149–157.
50. Iwai Y, Yamanaka K, Yasui T, et al. Gamma knife surgery for skull base meningiomas: the effectiveness of low-dose treatment. Surg Neurol 1999;52(1):40–44; discussion 44–45.
51. Saleh EA, Taibah AK, Achilli V, Aristegui M, Mazzoni A, Sanna M. Posterior fossa meningioma: surgical strategy. Skull Base Surg 1994;4(4):202–212.
52. Tsuruda JS, Chew WM, Moseley ME, Norman D. Diffusion-weighted MR imaging of the brain: value of differentiating between extraaxial cysts and epidermoid tumors. AJR Am J Roentgenol 1990;155(5):1059–1065; discussion 1066–1068.
53. Gulya AJ, Glasscock ME 3rd, Pensak ML. Neural choristoma of the middle ear. Otolaryngol Head Neck Surg 1987;97(1):52–56.
54. Nelson EG, Kratz RC. Sebaceous choristoma of the middle ear. Otolaryngol Head Neck Surg 1993;108(4):372–373.
55. Bottrill ID, Chawla OP, Ramsay AD. Salivary gland choristoma of the middle ear. J Laryngol Otol 1992;106(7):630–632.
56. Benecke JE Jr, Noel FL, Carberry JN, House JW, Patterson M. Adenomatous tumors of the middle ear and mastoid. Am J Otol 1990;11(1):20–26.
57. Guild SR. The glomus jugulare, a nonchromaffin paraganglion, in man. Ann Otol Rhinol Laryngol 1953;62(4):1045–1071; concld.
58. Spector GJ, Sobol S, Thawley SE, Maisel RH, Ogura JH. Panel discussion: glomus jugulare tumors of the temporal bone—patterns of invasion in the temporal bone. Laryngoscope 1979;89(10 Pt 1):1628–1639.
59. Yoo H, Jung HW, Yang HJ. Jugular foramen schwannomas: surgical approaches and outcome of treatment. Skull Base Surg 1999;9(4):243–252.
60. Som PM, Reede DL, Bergeron RT, Parisier SC, Shugar JM, Cohen NL. Computed tomography of glomus tympanicum tumors. J Comput Assist Tomogr 1983;7(1):14–17.
61. Larson TC 3rd, Reese DF, Baker HL Jr, McDonald TJ. Glomus tympanicum chemodectomas: radiographic and clinical characteristics. Radiology 1987;163(3):801–806.
62. Dichiro G, Fisher RL, Nelson KB. The jugular foramen. J Neurosurg 1964;21:447–460.
63. Olsen WL, Dillon WP, Kelly WM, Norman D, Brant-Zawadzki M, Newton TH. MR imaging of paragangliomas. AJR Am J Roentgenol 1987;148(1):201–204.
64. Hesselink JR, Davis KR, Taveras JM. Selective arteriography of glomus tympanicum and jugulare tumors: techniques, normal and pathologic arterial anatomy. AJNR Am J Neuroradiol 1981;2(4):289–297.
65. van Gils AP, van der Mey AG, Hoogma RP, et al. Iodine-123-metaiodobenzylguanidine scintigraphy in patients with chemodectomas of the head and neck region. J Nucl Med 1990;31(7):1147–1155.
66. Kwekkeboom DJ, van Urk H, Pauw BK, et al. Octreotide scintigraphy for the detection of paragangliomas. J Nucl Med 1993;34(6):873–878.
67. Krenning EP, Kwekkeboom DJ, Bakker WH, et al. Somatostatin receptor scintigraphy with [111In-DTPA-D-Phe1]- and [123I-Tyr3]-octreotide: the Rotterdam experience with more than 1000 patients. Eur J Nucl Med 1993;20(8):716–731.
68. Blake GB, Wilson JS. Malignant tumours of the ear and their treatment. I. Tumours of the auricle. Br J Plast Surg 1974;27(1):67–76.
69. Bird CR, Hasso AN, Stewart CE, Hinshaw DB Jr, Thompson JR. Malignant primary neoplasms of the ear and temporal bone studied by high-resolution computed tomography. Radiology 1983;149(1):171–174.
70. Michaels L, Wells M. Squamous cell carcinoma of the middle ear. Clin Otolaryngol Allied Sci 1980;5(4):235–248.
71. Oot RF, Melville GE, New PF, et al. The role of MR and CT in evaluating clival chordomas and chondrosarcomas. AJR Am J Roentgenol 1988;151(3):567–575.
72. Meyers SP, Hirsch WL Jr, Curtin HD, Barnes L, Sekhar LN, Sen C. Chordomas of the skull base: MR features. AJNR Am J Neuroradiol 1992;13(6):1627–1636.
73. Brooks JJ, LiVolsi VA, Trojanowski JQ. Does chondroid chordoma exist? Acta Neuropathol (Berl) 1987;72(3):229–235.
74. Grossman RI, Davis KR. Cranial computed tomographic appearance of chondrosarcoma of the base of the skull. Radiology 1981;141(2):403–408.
75. Bourgouin PM, Tampieri D, Robitaille Y, et al. Low-grade myxoid chondrosarcoma of the base of the skull: CT, MR, and histopathology. J Comput Assist Tomogr 1992;16(2):268–273.
76. Meyers SP, Hirsch WL Jr, Curtin HD, Barnes L, Sekhar LN, Sen C. Chondrosarcomas of the skull base: MR imaging features. Radiology 1992;184(1):103–108.
77. Batsakis JG, el-Naggar AK. Papillary neoplasms (Heffner's tumors) of the endolymphatic sac. Ann Otol Rhinol Laryngol 1993;102(8 Pt 1):648–651.
78. Megerian CA, McKenna MJ, Nuss RC, et al. Endolymphatic sac tumors: histopathologic confirmation, clinical characterization, and implication in von Hippel-Lindau disease. Laryngoscope 1995;105(8 Pt 1):801–808.
79. Ayadi K, Mahfoudh KB, Khannous M, Mnif J. Endolymphatic sac tumor and von Hippel-Lindau disease: imaging features. AJR Am J Roentgenol 2000;175(3):925–926.
80. Lo WW, Applegate LJ, Carberry JN, et al. Endolymphatic sac tumors: radiologic appearance. Radiology 1993;189(1):199–204.
81. Pulec JL. Facial nerve neuroma. Laryngoscope 1972;82(7):1160–1176.
82. Latack JT, Gabrielsen TO, Knake JE, et al. Facial nerve neuromas: radiologic evaluation. Radiology 1983;149(3):731–739.
83. Conley J, Janecka I. Schwann cell tumors of the facial nerve. Laryngoscope 1974;84(6):958–962.
84. Dort JC, Fisch U. Facial nerve schwannomas. Skull Base Surg 1991;1(1):51–56.
85. McMenomey SO, Glasscock ME 3rd, Minor LB, Jackson CG, Strasnick B. Facial nerve neuromas presenting as acoustic tumors. Am J Otol 1994;15(3):307–312.
86. Curtin HD, Jensen JE, Barnes L Jr, May M. "Ossifying" hemangiomas of the temporal bone: evaluation with CT. Radiology 1987;164(3):831–835.
87. Benoit MM, North PE, McKenna MJ, Mihm MC, Johnson MM, Cunningham MJ. Facial nerve hemangiomas: vascular tumors or malformations? Otolaryngol Head Neck Surg 2010;142(1):108–114.
88. Lo WW, Horn KL, Carberry JN, et al. Intratemporal vascular tumors: evaluation with CT. Radiology 1986;159(1):181–185.
89. Parker GD, Harnsberger HR. Clinical-radiologic issues in perineural tumor spread of malignant diseases of the extracranial head and neck. RadioGraphics 1991;11(3):383–399.
90. Arriaga M, Curtin HD, Takahashi H, Kamerer DB. The role of preoperative CT scans in staging external auditory meatus carcinoma: radiologic-pathologic correlation study. Otolaryngol Head Neck Surg 1991;105(1):6–11.
91. Nemzek WR, Hecht S, Gandour-Edwards R, Donald P, McKennan K. Perineural spread of head and neck tumors: how accurate is MR imaging? AJNR Am J Neuroradiol 1998;19(4):701–706.